ELSEVIER

Journal of Alloys and Compounds 229 (1995) 93–106

Journal of ALLOYS AND COMPOUNDS

Chemistry and properties of novel niobium cluster compounds

Gordon J. Miller

Department of Chemistry, Iowa State University, Ames, IA 50011, USA

Received 15 February 1995; in final form 21 March 1995

Abstract

Low-dimensional niobium chalcogenide halides provide interesting candidates for catalysis owing in part to their morphologies and electronic configuration. The synthesis, structures, properties, and electronic structures of novel compounds based on Nb_3 triangles and Nb_2 dimers are presented in this brief review. In addition, attempts at low temperature synthesis using organometallic precursors are discussed.

Keywords: Chemistry; Niobium cluster compounds

1. Introduction

Designing new materials with desirable and even well controlled properties is a major goal of synthetic solid state chemists and material scientists. Such properties include high temperature superconductivity, metallic conductivity at elevated temperatures ($T >$ 1500 °C), low-dimensional electronic or magnetic properties, good thermal stability, and exceptional catalytic activity, for example for hydrodesulfurization or hydrodenitrogenation [1]. Our recent efforts in the field of materials design include utilizing low nuclearity early transition metal clusters, for example with niobium or tantalum, in low-dimensional morphologies to provide a class of materials that may prove useful as either heterogeneous catalysts or low-dimensional electronic devices.

This brief account summarizes our experimental and theoretical investigations of low-dimensional niobium chalcogenide halides, which contain dimers and trimers of niobium atoms. Our major goal is to design a compound, or series of compounds, whose structure contains available space into which small molecules may diffuse, and involves a framework that offers some electronic flexibility. This contribution specifically outlines the rationale for selecting niobium chalcogenide halides for our initial investigations and some of our most interesting results in synthetic design and solid state chemistry of these materials.

The account is organized as follows. Section 2 introduces our rationale by briefly reviewing both the chemistry of niobium halides as well as the nature of interactions between transition metals and chalcogen atoms. Section 3 describes the solid state synthetic strategies. Section 4 summarizes some observations and new theoretical results in the binary Nb_3X_8 and ternary Nb_3YX_7 family of compounds (X ≡ Cl, Br, I; Y ≡ S, Se, Te). Section 5 details our surprising results in the Nb–S–I system, and Section 6 introduces our efforts with metal–organic reagents as precursors to novel inorganic solids.

2. Background

Niobium halides from a rich collection of cluster compounds—perhaps the most diverse set of structures and oxidation states of any transition metal halide system [2]. Moreover, not only do they exhibit different cluster geometries, but their long-range morphologies span molecular structures of three-dimensional networks. Thus, with potential chemical and physical applications in mind, niobium halides offer electronically diverse centers, accessible cavities for guest species, and sufficient structural rigidity and electronic stability to accommodate diffusion of small molecules.

Table 1 lists several binary halides of niobium and some salient features. The d^0 pentahalides are all molecular solids consisting of two edge-sharing octa-

Table 1
Summary of structural and electronic features of solid state niobium halides, CVE cluster valence electrons

Compound	Structural formula	Nb_n Clusters	CVE	Remarks	Reference
Chlorides					
$NbCl_5$	$[NbCl_4Cl_{2/2}]_2$	—	0	Nb···Nb 3.929 Å	3
$NbCl_4$	$^1_\infty[NbCl_2Cl_{4/2}]_2$	···Nb–Nb···	2	Nb–Nb 3.029, 3.794 Å; diamagnetic	4
Nb_3Cl_8 (α)	$^2_\infty[NbCl_{1/3}Cl_{2/2}Cl_{2/2}Cl_{1/3}]_3$	Nb_3 triangles	7	Nb–Nb 2.81 Å; $\mu_{298} = 1.86\ \mu_B$ $Nb_{3-x}Cl_8$ ($x \leq 0.44$)	5
Nb_6Cl_{14}	$^3_\infty[Nb_6Cl_{10}Cl_{2/2}]Cl_{2/2}Cl_{4/2}$	Nb_6 octahedra	16	⟨Nb–Nb⟩ 2.91 Å; weak paramagnetic	6
Bromides					
$NbBr_5$	$[NbBr_4Br_{2/2}]_2$	—	0	Nb···Nb 4.157 Å	7
$NbBr_4$	$^1_\infty[NbBr_2Br_{4/2}]_2$	···Nb–Nb···	2	Nb–Nb 3.029, 3.794 Å; diamagnetic	8
Nb_3Br_8 (α)	$^2_\infty[NbBr_{1/3}Br_{2/2}Br_{2/2}Br_{1/3}]_3$	Nb_3 triangles	7	$Nb_{3-x}Br_8$ ($x \leq 0.36$)	9
Nb_3Br_8 (β)	$^2_\infty[NbBr_{1/3}Br_{2/2}Br_{2/2}Br_{1/3}]_3$	Nb_3 triangles	7	Nb–Nb 2.88 Å; $\mu_{298} = 0.73\ \mu_B$	10
Iodides					
NbI_5	$[NbI_4I_{2/2}]_2$	—	0	Nb···Nb 4.499 Å	11
NbI_4	$^1_\infty[NbI_2I_{4/2}]_2$	···Nb–Nb···	2	Nb–Nb 3.029, 3.794 Å	12
Nb_3I_8 (α)	$^2_\infty[NbI_{1/3}I_{2/2}I_{2/2}I_{1/3}]_3$	Nb_3 triangles	7	$Nb_{3-x}I_8$ ($0.23 \leq x \leq 0.38$)	9
Nb_3I_8 (β)	$^2_\infty[NbI_{1/3}I_{2/2}I_{2/2}I_{1/3}]_3$	Nb_3 triangles	7	Nb–Nb 288 Å; $\mu_{298} = 0.73\ \mu_B$	10
NbI_3	$^1_\infty[NbI_{6/2}]$	$^1_\infty[-Nb-]$	4	Hexagonal	13
Nb_6I_{11}	$^3_\infty[Nb_6I_8]I_{6/2}$	Nb_6 Octahedra	19	⟨Nb–Nb⟩ 2.853 Å; LT; $S = 1/2$ ⟨Nb–Nb⟩ 2.847 Å; HT; $S = 3/2$	14

hedra, $[NbX_4X_{2/2}]_2 \equiv Nb_2X_{10}$. Coulomb interactions between the Nb(V) ions effect a shift away from the molecular center and essentially no Nb–Nb bond (distances greater than 3.5 Å). The d^1 tetrahalides are all linear chain compounds, based on trans edge-sharing octahedra, $^1_\infty[NbX_2X_{4/2}] \equiv NbX_4$. These compounds are diamagnetic owing to a formal Nb–Nb single bond, because Nb–Nb bond alternation (—short—long—) occurs along each chain. Note that matrix effects, i.e. the halide, influences the short Nb–Nb distances in these compounds. The more reduced niobium halides no longer show integral oxidation states. For example, no stoichiometric d^2 NbX_3 has been well characterized (note, NbI_3 is mentioned in various publications without detailed characterization [13]), but for both the chloride and bromide systems, this stoichiometry is part of a homologous series α-NbX_x ($2.67 \leq x < 3.2$) [15]. At the lower limit of x, the resulting α-Nb_3X_8 structures adopt a defect CdI_2-type arrangement that contains Nb_3 triangles. Strong Nb–Nb bonding in this cluster results in one unpaired electron per Nb_3 cluster [10]. Finally, the compounds NbX_2 are unknown, but Nb_6Cl_{14} and Nb_6I_{11} represent line compounds that consist of either Nb_6Cl_{12} edge-capped or Nb_6I_8 face-capped metal octahedra. Unlike their more oxidized counterparts, these reduced niobium halides are coordinated by five halides in a square pyramidal arrangement: four occupy *innen* positions of the cluster and the fifth occupies an *ausser* position. (See Ref. [2], *innen* is *interior* to the cluster, *ausser* is *exterior* to the cluster.) Again, the Nb–Nb bonding is sufficiently strong so as to minimize the number of unpaired electrons in these clusters. Fig. 1 illustrates some of these niobium clusters. To summarize these observations on a well investigated series of compounds, (1) niobium halide structures generally involve close packings of halides with Nb atoms in octahedral holes, (2) for d counts greater than 2.5 electrons per Nb atom, Nb–Nb bonding can replace Nb–X bonding, and (3) Nb–Nb interactions are paramount to providing nonmetallic characteristics.

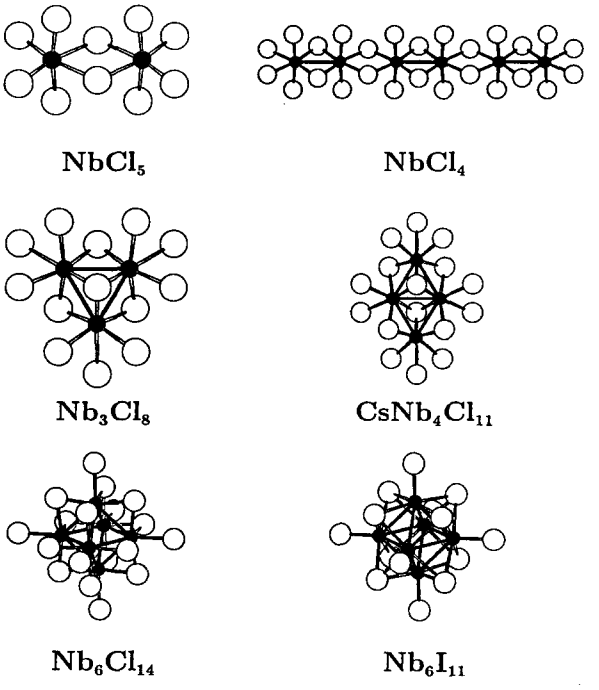

Fig. 1. Cluster units in various niobium halides: filled circles, Nb; open circles, halide.

The other aspect of our problem concerns metal–

chalcogenide interactions and how they correlate with the existence of polychalcogenide anions in these solids. In a recent review, Rouxel points out the intricate charge transfer characteristics that can occur in these compounds [16]. Using the transition metal dichalcogenide structures as a basis, as the electronegativity of the metal decreases, there is greater tendency toward catenation of the chalcogen atoms, cf. MoS_2 (molybdenite-type) vs. RuS_2 (pyrite-type). In other words, early transition metals show evidence for greater electron transfer to the chalcogen: M(IV) oxidation states, no S–S contacts, and layered arrangements based on CdI_2 (TiS_2) or MoS_2. The later transition metals, however, occur as M(II) ions with disulfide groups in the pyrite structure.

The Mulliken recipe for electronegativity of atoms, which is $\chi(\text{Mulliken}) \propto (\text{IP(I)} + \text{EA})/2$ (IP(I) is the first ionization potential, EA is the electron affinity) [17], allows generalization to ions, and it becomes clear that for a given atom, the electronegativity increases with oxidation states. Therefore, for the early transition metals, any internal redox chemistry between the metal and chalcogen becomes increasingly relevent as the oxidation state of the metal increases. Consider niobium as an example. NbS_2, isotypic to MoS_2, is formulated as $Nb^{4+}(S^{2-})_2$. However, NbS_3 cannot be written as an Nb^{5+} compound [15]. It is, in fact, formulated as $Nb^{4+}(S_2)^{2-}(S^{2-})$. Nb_2S_5 is an unknown phase in the Nb–S phase diagram, although low temperature routes using organic sulfurizing reagents have led to products with this composition [18,19]. IR spectra do not show any evidence for $(S–S)^{2-}$ groups, although the formulation $(Nb^{4+})_2(S_2)^{2-}(S^{2-})_3$ would be expected according to the previous arguments. Ternary niobium chalcogenide halides have also demonstrated this type of "internal redox chemistry", in for example $NbSeBr_3$, which is $(Nb^{4+})_2(Se–Se)^{2-}(Br^-)_6$ with an Nb–Nb single bond rather than a d^0 Nb(V) center. Table 2 summarizes some of the geometrical data for these ternary compounds and Fig. 2 illustrates how the dichalcogenide groups interact with the metal centers.

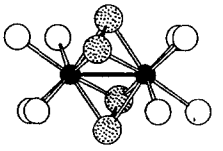

$NbSe_2Cl_2$

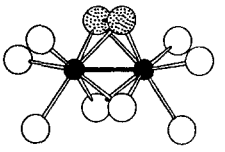

$Nb_2Se_2Br_6$

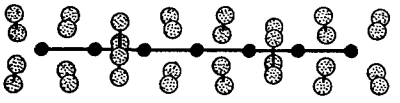

$NbSe_4I_{0.33}$

Fig. 2. Fundamental structural groups in ternary niobium chalcogenide halides: filled circles, Nb; dotted circles, chalcogenide; open circles, halide.

Table 2
Summary of structural features of solid state niobium chalcogenide halides Nb–Y–X (Y = chalcogen, X = halogen)

Compound	Ionic formulation	Nb–Nb (Å)	Nb–Y (Å)	Nb–X (Å)	Y–Y (Å)	Reference
NbS_2Cl_2	$(Nb^{4+})(S_2)^{2-}(Cl^-)_2$	2.87	2.49	2.60	2.00	21
Nb_6Si_9	$(Nb_6)^{11+}(S^{2-})(I^-)_9$	2.90	2.46	2.86	–	22
$NbSe_2Cl_2$	$(Nb^{4+})(Se_2)^{2-}(Cl^-)_2$	2.97	2.62	2.59	2.27	21
$Nb_3Se_5Cl_7$	$(Nb^{5+})(Nb^{4+})_2(Se_2)_2^{2-}(Se^{2-})(Cl^-)_7$	2.94	2.25, 2.61	2.49, 2.60	2.30	23
$Nb_2Se_2Br_6$	$(Nb^{4+})_2(Se_2)^{2-}(Br^-)_6$	2.83	2.61	2.66	2.31	20
$Nb_6Se_{20}Br_6$	$(Nb^{4.33+})_6(Se_2)_{10}^{2-}(Br^-)_6$	3.10	2.60	2.70	2.33	24
$Nb_3Se_{20}Br_2$	$(Nb^{4+})_3(Se_2)_5^{2-}(Br^-)_2$	3.17	2.64	2.60	2.31	25
$Nb_4Se_{16}Br_2$	$(Nb^{4.5+})_4(Se_2)_8^{2-}(Br^-)_2$	3.15	2.70	–	2.31	26
$NbSe_2Br_2$	$(Nb^{4+})(Se_2)^{2-}(Br^-)_2$	2.96	2.61	2.77	2.29	27
$NbSe_4I_{0.33}$	$(Nb^{4.33+})(Se_2)_2^{2-}(I^-)_{0.33}$	3.06	2.66	–	2.36	28
NbSeI	$(Nb^{3+})(Se^{2-})(I^-)$	2.97	2.55	3.00	–	29, 30
$Nb_2Te_2Br_6$	$(Nb^{4+})_2(Te_2)^{2-}(Br^-)_6$	2.88	2.85	2.66	2.67	20
$Nb_2Te_2I_6$	$(Nb^{4+})_2(Te_2)^{2-}(I^-)_6$	2.93	2.83	2.90	2.69	20
$Nb_4Te_{12}I_2$	$(Nb^{4+})_4(te_2)_5^{2-}(Te^{2-})_2(I^-)_2$	2.83–3.24	2.90	2.86	2.78	31
$Nb_4Te_{12}I$	$(Nb^{4.25+})_4(Te_2)_4^{2-}(Te^{2-})_4(I^-)$	3.05	2.85	3.00	2.71	32
$NbTe_4I$	$(Nb^{5+})(Te_2)_4^{2-}(I^-)$	–	2.85	–	2.79	33

As the table shows, most compounds involve Nb(IV) ions.

Our working hypothesis involves probing the capacity of ternary niobium chalcogenide halides towards various catalytic applications. The rationale comes by combining the two ideas promoted in the previous paragraphs: (1) niobium displays a diverse cluster chemistry that varies with oxidation state; (2) various oxidation states should lead to internal redox chemistry when chalcogen atoms, i.e. S, Se, Te, are included. As both Tables 1 and 2 demonstrate, this chemistry will be most interesting for Nb(III)–Nb(IV) systems. In other words, we are designing chemical systems that offer electronic flexibility through both metal–metal bonded clusters and partially oxidized anion fragments. In order to serve as catalysts, we need morphologies that allow appropriate space for the molecules involved in the catalytic processes, in particular layered compounds and open framework structures. This review summarizes recent results involving the solid state chemistry of layered niobium halides and chalcogenide halides.

3. Synthetic strategies

Solid state synthetic procedures for binary niobium chalcogenides and halides include numerous high and low temperature approaches [34]. Certainly, in order to obtain single crystals suitable for X-ray diffraction experiments, chemical vapor transport has been extensively and successfully used to prepare these compounds [35]. Such reactions involve a solid substance A reacting with a gas $B^{(k)}$ to form exclusively gaseous phase products $C^{(j)}$, which undergo the reverse reaction somewhere else in the system;

$$iA_{(s)} + kB^{(k)}_{(g)} + \cdots = jC^{(j)}_{(g)} + \cdots .$$

In addition to a reversible heterogeneous reaction, there must exist a concentration gradient, which can result from a temperature gradient, a difference in relative partial pressures, or a difference in the free energy of formation of two substances. For the layered niobium halides, reactions are carried out in closed ampoules, and the concentration gradient is formed via a temperature gradient. The different temperatures control the partial pressures of gaseous components, and as long as there is a significant difference in partial pressures for $C^{(j)}_{(g)}$, transport can take place. The direction of transport is therefore dictated by the enthalpy of the reaction above: if $\Delta H > 0$ (endothermic), transport occurs from high to low temperature; if $\Delta H < 0$ (exothermic), transport occurs from low to high temperature. In general, the equilibrium conditions occur much faster than diffusion, which controls transport rates. As a general rule, $\Delta P_j / \Sigma P > 10^{-4}$ is desirable for the diffusing species; K_p should be neither too large nor too small at the operating temperatures.

Nb_3Br_8 and Nb_3I_8 have been prepared from the elements [10], whereas Nb_3Cl_8 is obtained by an appropriate mixture of Nb metal and $NbCl_5$ [5]. Owing to the presence of more reduced Nb halides in each system, the reaction containers are generally fused silica and the temperature conditions range between 800 and 1100 K. Based on the two different approaches, the heterogeneous equilibria that contribute to chemical transport are

$$Nb_3Cl_{8(s)} + 4NbCl_{5(g)} \rightleftharpoons 7NbCl_{4(g)}$$

$$Nb_3I_{8(s)} + 2I_{2(g)} \rightleftharpoons 3NbI_{4(g)}$$

As written, both equilibria have $\Delta H < 0$, so that transport of the solid phase is carried out from lower to higher temperature within the reaction container.

The halide phases at this stoichiometry have been extensively studied to show that the composition of the solid depends on the composition of the gas phase [35]. In particular, the following homogeneity ranges have been observed [15]: $NbCl_{2.67\cdots3.13}$ ($Nb_{3-x}Cl_8$, with $x \leq 0.44$); $NbBr_{2.67\cdots3.03}$ ($x \leq 0.36$); $NbI_{2.89\cdots3.05}$ ($0.23 \leq x \leq 0.38$). Owing to the variable composition of the solid phase, the general transport reactions are

$$NbCl_{x(s)} + (4-x)NbCl_{5(g)} \rightleftharpoons (5-x)NbCl_{4(g)}$$

$$NbBr_{x(s)} + (4-x)NbBr_{5(g)} \rightleftharpoons (5-x)NbBr_{4(g)}$$

$$2NbI_{x(s)} + (1-x)I_{2(g)} \rightleftharpoons 2NbI_{4(g)}$$

Therefore, for a specific temperature, the composition of the solid phase can be adjusted by fixing either the pentahalide or halogen equilibrium pressure. Visual and X-ray inspection of the products reveals homogeneous preparations in the chloride system as the crystals vary from green ($NbCl_{2.67}$) to brown ($NbCl_{3.13}$).

Chemical transport is also important for the synthesis of niobium chalcogenide halides but, as anticipated, the equilibria for these ternary systems are more complex than for the binary halides. In fact, halogens such as I_2 and Br_2, as well as halides such as $NbCl_5$ and $NbBr_5$, can serve as effective transport agents for the synthesis, purification, and crystallization of binary chalcogenides. To our knowledge, these equilibria have not been studied in detail. Nevertheless, our efforts have revealed that such heterogeneous equilibria do occur in the Nb–S–I ternary system. Above ca. 990 K, S_2 is the predominant sulfur species in the gas phase, and at lower pressures it is the most prominent species above 800 K [36]. We have found that for temperatures below 1100 K, the following reaction occurs:

$$7Nb_{(s)} + S_{2(g)} + \frac{19}{2} I_{2(g)} \xrightarrow[48\ h]{1100\ K} Nb_7S_2I_{19(s)}$$

with the solid phase product condensing throughout the ampoule. However, at higher temperatures ($T > 1100$ K), we do not observe this particular product, but detect $Nb_{14}S_5$ via powder X-ray diffraction. This can form according to the following proposed equilibrium:

$$2Nb_{14}S_{5(s)} + 56I_{2(g)} \rightleftharpoons 28NbI_{4(g)} + 5S_{2(g)}$$

The synthesis and characterization of numerous niobium chalcogenide halides have been reported for mostly Nb(IV) compounds. Examples include NbS_2Cl_2, $NbSCl_3$ (equivalent to $Nb_2S_2Cl_6$), and $NbSe_4I_{0.33}$. There are relatively few reports of this chemistry for any reduced niobium systems, and we have concentrated our initial efforts towards an understanding of the solid state chemistry of systems constructed from Nb_3 triangular clusters. The last section of this review addresses our efforts using metal–organic precursors for inorganic solids and we address certain synthetic strategies there.

4. The Nb_3X_8 system

The three binary halides Nb_3X_8 ($X \equiv Cl$, Br, I) have been known for almost three decades [5,10]. Two crystallographically distinct structures occur which differ in the stacking pattern of two-dimensional building blocks. They are layered materials and resemble CdI_2 or $CdCl_2$ in that octahedral holes in alternate layers of close packed halide ions are occupied by niobium ions. They represent, in fact, defect CdI_2 or $CdCl_2$ structures as only three-quarters of the octahedral holes within a given layer are occupied: $^2_\infty[Nb_3\square_1X_8]$. The arrangement of occupied interstices leads to Nb_3 triangles with one capping halide ion (see top of Fig. 3). The two variants are identified by their mode of anion packing as well as the cation distribution, which dictates the ultimate space group: the α-form, with the $\cdots$h$\cdots$ mode (hexagonally close packed anion array), has space group $P\bar{3}m1$; and the β-form, with the $\cdots$hhcc$\cdots$ mode (50:50 mixture of hexagonally and cubic close packed), has space group $R\bar{3}m$. In terms of the ABC scheme, which denotes the three possible sites in the two-dimensional hexagonal

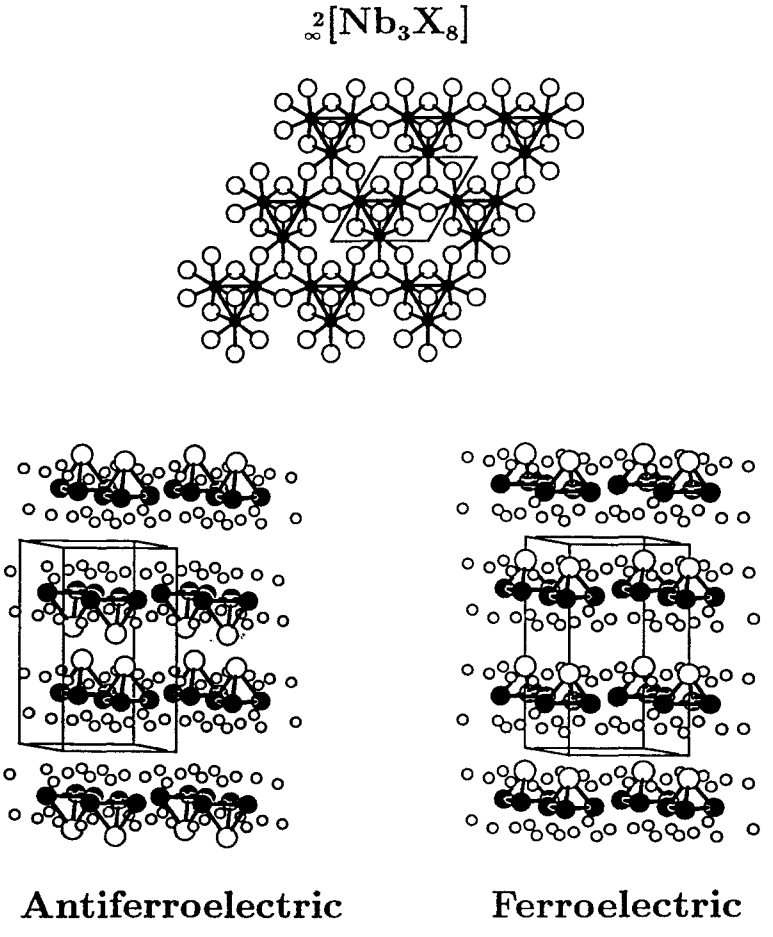

Fig. 3. Top, (001) projection of a single $^2_\infty[Nb_3X_8]$ layer. This layer leads to two of many morphologies, which are categorized as either antiferroelectric (α-Nb_3Cl_8, $P\bar{3}m1$) or ferroelectric (Nb_3SeI_7, $P6_3mc$).

projection of any close packing, these two schemes are [37]

$\cdots h \cdots \equiv \cdots AB \cdots$

$\cdots hhcc \cdots \equiv \cdots ABCBCABABCAC \cdots$

Both space groups are centrosymmetric. Since the two-dimensional building block does not have an inversion center, this symmetry operation must be generated by how these layers stack with respect to each other. In fact, if we concentrate on the tetrahedron formed by the three Nb atoms and the capping halide **1**, within a $^{2}_{\infty}[Nb_3X_8]$ layer each tetrahedron is oriented parallel with one another: a ferroelectric arrangement. The only way of producing an inversion center is to develop antiferroelectric packing of these layers (see also Fig. 3). The inversion center, therefore, lies in the van der Waals gaps.

The halides Nb_3X_8 have also been physically characterized and may be classified as magnetic semiconductors. α-Nb_3Cl_8 exhibits a Curie–Weiss behavior in its magnetic susceptibility with $\mu_{eff} = 1.86\ \mu_B$, which is appropriate for one unpaired electron. This result is consistent with simple electron counting: $Nb_3Cl_8 \equiv (Nb_3)^{8+}(Cl^-)_8$, which gives seven electrons for Nb–Nb bonding. Six of these electrons are assigned to three two-center-two-electron Nb–Nb bonds in the triangle, which leaves one unpaired electron. β-Nb_3Br_8 and β-Nb_3I_8 also show paramagnetic behavior, but values of their effective magnetic moments are significantly lower than the spin-only value. Although these magnetic data have been attributed to superexchange mechanisms via the bridging halides [38], the detailed mechanism of magnetic exchange has yet to be elucidated. All are intrinsic semiconductors with thermal activation energies (band gaps) of approximately 0.1–0.2 eV [39].

Let us now consider a description of the Nb_3X_8 structure from a molecular perspective. Each two-dimensional layer is composed of condensed $[Nb_3X_{13}]^{5-}$ clusters according to the formula $[Nb_3XX'_3X''_{6/2}X'''_{3/3}]$ (**2**). X is the capping anion, X′ atoms bridge each edge of the triangle, X″ bridge two clusters, and X‴ connect three triangles. These Nb_3X_{13}

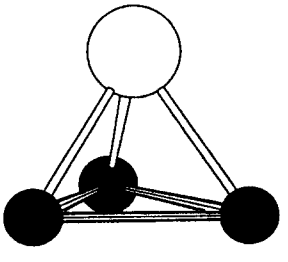

1

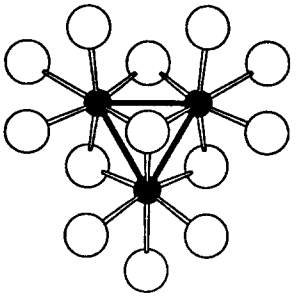

2

units are well known to show cluster valence electron counts between six and eight electrons. Some examples include $[Nb_3Cl_{10}(PEt_3)_3]^-$ (six electrons) [40] and $Nb_3Cl_7(PMe_2Ph)_6$ (eight electrons) [40].

Several molecular orbital and band structure calculations have been carried out on the $[Nb_3X_{13}]^{n-}$ cluster anions [41] as well as the Nb_3X_8 sheets [42]. Although there are some subtle differences between the calculated spectra of the molecules and the extended solid, the basic pattern of levels (bands) arises by sequentially turning on Nb–ligand and then Nb–Nb interactions. Since each Nb atom is octahedrally coordinated, the 4d orbitals are split into a t_{2g} and an e_g set; the threefold degenerate set is crucial for the observed electron counts. When Nb–Nb interactions are included, these levels are split into three sets of three levels that may be assigned qualitatively as Nb–Nb bonding, non-bonding, and antibonding. Fig. 4 illustrates the patterns for the isolated molecular anion $[Nb_3X_{13}]^{n-}$ and the average band positions for

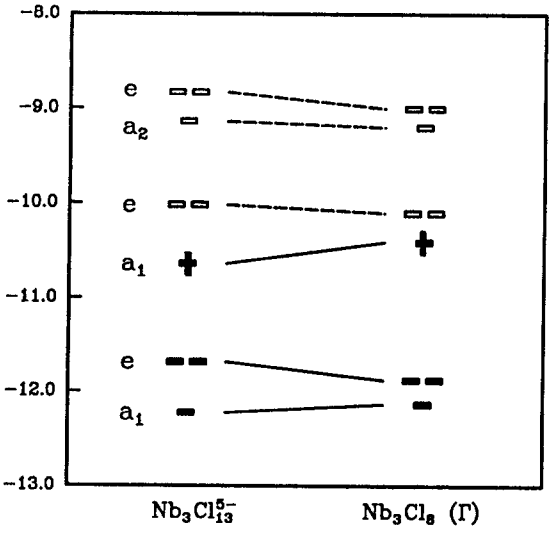

Fig. 4. Molecular orbital energy correlation of the valence Nb 4d orbitals between (left) an isolated $[Nb_3Cl_{13}]^{5-}$ cluster, and (right) the $^{2}_{\infty}[Nb_3Cl_8]$ sheet (evaluated at the Γ point (0, 0) in reciprocal space).

$^2_\infty[Nb_3Cl_8]$. Extended Hückel calculations on $Nb_3Cl_7(PMe_2Ph)_6$ and the $[Nb_3Cl_{13}]^{5-}$ cluster isolated from Nb_3Cl_8 give a HOMO-LUMO gap of ca. 0.55 eV. In the two-dimensional layer compound Nb_3Cl_8, translational symmetry introduces the wavevectors $\boldsymbol{k}$ as an additional symmetry label and discrete orbitals are broadened into bands. The intercluster orbital interactions are mediated by two sets of bridging chlorides, and for the set of levels near the Fermi level for α-Nb_3Cl_8, this overlap is extremely weak. Thus, these bands are narrow and behave as localized molecular orbitals. However, the gap between the highest occupied (a_1) and lowest unoccupied crystal orbital (e) is now 0.3 eV [43].

Surprisingly, α-Nb_3X_8 represents the end member of a homologous series of compounds near the stoichiometry NbX_3 for each halide. However, the rhombohedral β-forms for the bromide and iodide are stoichiometric Nb_3X_8 and show no homogeneity width. To data there exists no explanation for this observation. Within the α-halides, Nb_3X_8 represents the most reduced Nb, and an alternative description for this homologous series is $Nb_{3-x}X_8$, where $0 \leq x < 0.5$. According to Hulliger [15], this series may be described as a solid solution of Nb_3 triangles and Nb_2 dimers within the halide matrix. Using this picture, we can describe the series as $(Nb_3)_{1-x}(Nb_2)_xX_8$ (x has the same meaning as earlier in this paragraph). Therefore, the ratio of Nb_2 dimers to Nb_3 trimers along this series can vary from 0 to 1 (the ratio varies as $x/1-x$). From a theoretical perspective, the complex system of two components x Nb_2Cl_8:$(1-x)$ Nb_3Cl_8 requires use of the grand canonical ensemble, which maintains equal chemical potentials (Fermi levels) between the two components [44]. Under this condition, our electronic structure calculations indicate that electron transfer will take place from the $(Nb_3)^{8+}$ trimers to the $(Nb_2)^{8+}$ dimers [43]. Fig. 5 illustrates the average energies for the valence bands (cluster orbitals) of the trimer and dimer, and each level's Nb–Nb contribution to the overlap population [45] is indicated. Clearly, the HOMO of the Nb_3 triangle will be depleted and the Nb_2 δ^* orbital will accept electrons. Therefore, the dimer can undergo significant reduction without substantial effects on the total Nb–Nb bonding. As the Nb_2:Nb_3 ratio increases, the Nb_3 triangles must become increasingly oxidized. Near the value unity, we find that the Nb–Nb bonding states for the Nb_3 unit must be depleted according to the calculated Fermi level. At or near this point, $Nb_{3-x}X_8$ would rather disproportionate into NbX_4 and a more reduced niobium halide (Nb_6X_{14} or Nb_6X_{11}). Thus, the thermodynamic stability of this entire series is derived from how the electronic states of the two clusters in the same chemical system interact with each other via electron transfer.

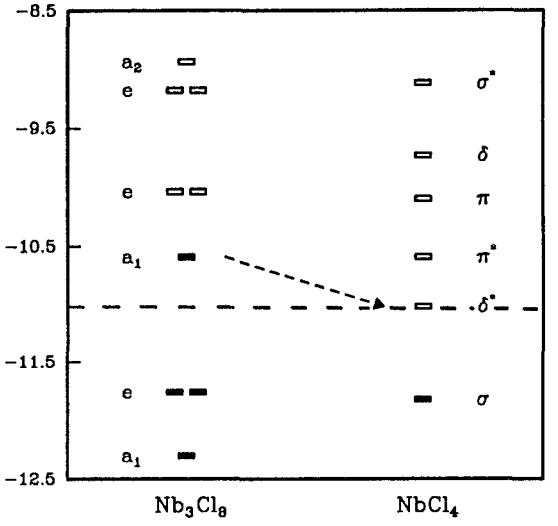

Fig. 5. Comparison of the average valence band (Nb 4d orbitals) energies for (left) $^2_\infty[Nb_3Cl_8]$ and (right) $^2_\infty[Nb_2Cl_8] \equiv {}^1_\infty[NbCl_4]$. Charge transfer is indicated by the arrow and the dashed line represents an "averaged" fermi level for $Nb_{3-x}Cl_8 \equiv (Nb_3)_{1-x}(Nb_2)_xCl_8$.

Crystallographically, the $^2_\infty[Nb_3X_8]$ layer offers four inequivalent sites: (1) μ_3-X capping the triangle ($\mu_3 - X^i$); (2) $\mu_2 - X$ bridging each edge of the cluster ($\mu_2 - X^i$); (3) $\mu_2 - X$ bridging two clusters ($\mu_2 - X^{a-a}$); (4) $\mu_3 - X$ bridging three triangles ($\mu_3 - X^{a-a}$), in which we use the innen and ausser notation developed by Schäfer and Schnering [2]. We can, therefore, represent these compounds as $[NbX^i_{1/3}X^i_{2/2}X^{a-a}_{2/2}X^{a-a}_{1/3}]_3$. Ternary derivatives of the binary halides offer a site preference problem owing to the different site potentials arising at the anion positions. According to the rule of topological charge stabilization [46], more electronegative components will occupy sites that have greater electron densities which, within the context of extended Hückel theory, may be estimated using a Mulliken population analysis. For $^2_\infty[Nb_3Cl_8]$ we find the following distribution in populations: $\mu_3 - Cl^i$, 6.735; $\mu_2 - Cl^i$, 6.801; μ_2-Cl^a, 7.303; $\mu_3 - Cl^a$, 7.220. Thus, the $\mu_3 - X^i$ position in the $^2_\infty[Nb_3X_8]$ layer is the preferred site for substitution by the more electropositive chalcogens.

Indeed, we and others have found that one halide can be successfully replaced by a chalcogen atom to give the new compounds Nb_3YX_7 ($Y \equiv S$, Se, Te; $X \equiv Cl$, Br, I). In every case, this atom substitutes at the $\mu_3 - X^i$ capping site in the $^2_\infty[Nb_3X_8]$ layer. Since there are no Y–Y bonds in these materials, each Nb_3 cluster will have six valence electrons and these ternary compounds will be diamagnetic semiconductors. Structural data are summarized in Table 3. Note that the more oxidized clusters in Nb_3YX_7 show larger Nb–Nb distances to indicate that the HOMO of the seven-electron cluster is somewhat Nb–Nb bonding.

Table 3
Various structural features for compounds Nb_3YX_7

Compound	Space group	Stacking variant	Nb–Nb (Å)	Nb–Y (Å)	Nb–X (Å)
Nb_3Cl_8	$P\bar{3}m1$	···h···	2.809	2.462	2.424–2.624
Nb_3TeCl_7	$P\bar{3}m1$	···h···	2.897	2.699	2.414–2.674
Nb_3Br_8	$R\bar{3}m$	···hhcc···	2.882	2.596	2552–2.792
Nb_3SBr_7	$P\bar{3}m1$	···h···	2.901	2.416	2.544–2.805
Nb_3SeBr_7 [a]	$P\bar{3}m1$	···h···	3.010	2.520	2.530–2.820
Nb_3TeBr_7	$P\bar{3}m1$	···hc···	2.958	2.702	2.557–2.819
Nb_3I_8	$R\bar{3}m$	···hhcc···	3.002	2.755	2.756–3.020
Nb_3SI_7	$P6_3mc$	···hc···	2.995	2.404	2.737–2.993
Nb_3SeI_7	$P6_3mc$	···hc···	3.017	2.533	2.716–3.002
Nb_3TeI_7	$p6_3mc$	···hc···	3.040	2.695	2.722–3.001

[a] X-ray powder diffraction.

After the identification of an Nb_3X_8-type X-ray powder pattern following the thermal decomposition of $Nb_2Te_2I_6$ [20] there have been numerous attempts to synthesize ternary derivatives of these binary halides. Furuseth and Hönle were the first to synthesize successfully and to characterize structurally Nb_3TeBr_7 [47], which required analysis of twinned crystal data in order to establish its three-dimensional structure. In the meantime, nearly all ternary Nb_3XY_7 have been characterized structurally, some requiring twinned crystal analysis. Single crystals of Nb_3TeCl_7 could be prepared by heating Nb foil, Te powder, and $NbCl_5$ powder to 1073 K for 1 week followed by rapid quenching to room temperature [43]. Such crystals were dark hexagonal plates and a good example gave the diffraction patterns in Fig. 6 (X-ray precession photographs; $l = 0$ and $h + k = 0$ layers).

Although the two-dimensional sheet remains intact, these ternary derivatives manifest new stacking arrangements, most of which represent a ferroelectric mode of stacking (see Fig. 3). There are now five different variations observed for the Nb_3YX_7 structures: (1) α-Nb_3Cl_8-type [5]; (2) β-Nb_3I_8-type [10]; (3) Nb_3TeBr_7-type [47], (4) Nb_3SeI_7-type [47]; (5) Nb_3Sbr_7-type [47,48]. The first two are centrosymmetric and the other three are non-centrosymmetric. Although reasons for the different morphologies remain unknown, Fig. 7 shows that these different stacking variants can be separated using a structure sorting diagram which utilizes the Pauling electronegativities of the two different anions as the sorting parameters. Lattice energy calculations, which include Madelung, Born–Mayer, and van der Waals terms, have been carried out for the various models using Nb_3TeCl_7 as the geometrical prototype [43]. Although these calculations were successful for this system, it is still not clear what factors dictate the different stacking arrangements.

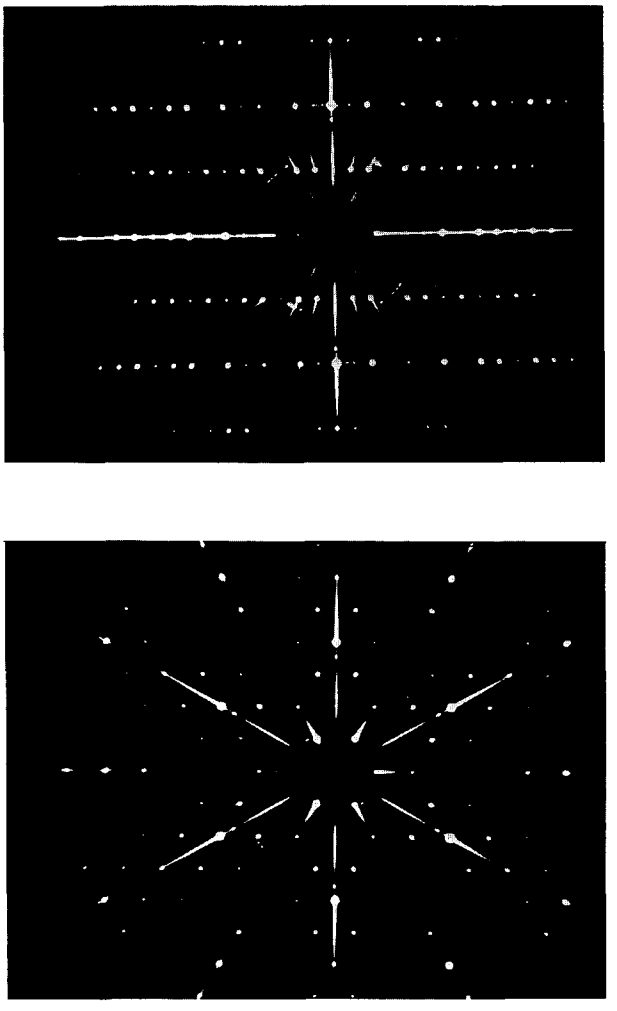

Fig. 6. X-ray precession photographs for a single crystal of Nb_3TeCl_7: $l = 0$ projection (left); $h + k = 0$ projection (right).

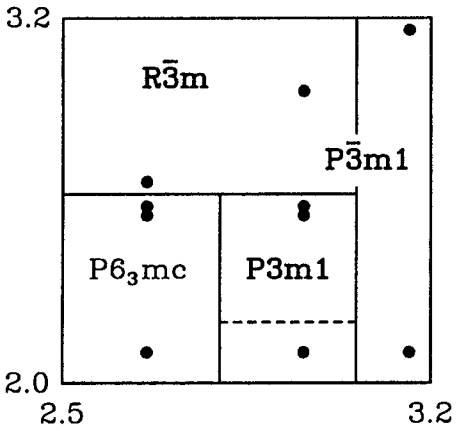

Fig. 7. Structure sorting plot for Nb_3YX_7-type compounds. The scales for the abscissa (X atoms) and ordinate (Y atoms) are Pauling electronegativities; Y ≡ S, Se, Te, Cl, Br, I; X ≡ Cl, Br, I. The *P3m1* field contains two different stacking variants separated by the dashed line.

5. The remarkable Nb–S–I system

According to Fig. 7, there is a demarcation between the centrosymmetric $R\bar{3}m$ structure of Nb_3I_8 and the non-centrosymmetric $P6_3mc$ structure of Nb_3SI_7, although the electronegativity difference between sulfur and iodine is small. This observation led us to investigate the Nb–S–I system near the stoichiometry Nb_3SI_7 with increased vigor owing to the potential electronic similarity of sulfur and iodine, but with clear size and charge differences. In these layered compounds, niobium occurs as formally Nb(III). Therefore, in a general study of $Nb(III)/S^{2-}/I^-$, Nb_3SI_7 is one example of the general set NbS_sI_i, where $2s + i = 3$ (**3**). In addition to the Nb_3X_8 derivatives, we have examined "NbSI" as a potential analog to NbSeI [29,30]. Our results in this section of the ternary phase diagram of niobium, sulfur, and iodine reveal that these ternary systems are open to an extremely diverse chemistry. In this section, we summarize three of our most recent results.

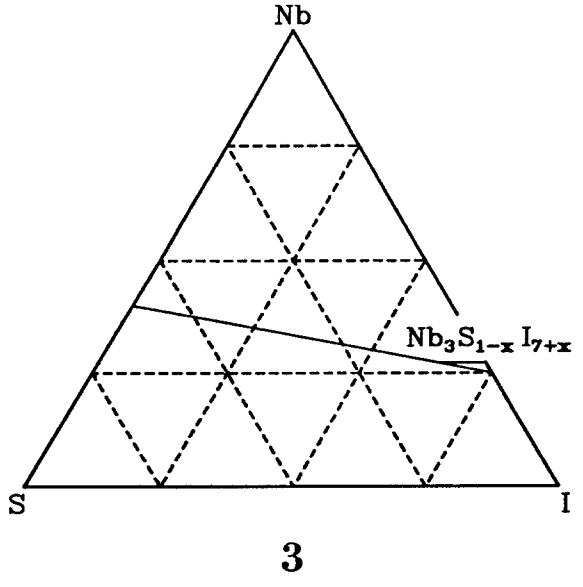

3

5.1. Orthorhomic Nb_3Si_7

Our initial detailed investigations of the Nb–S–I system near "Nb_3SI_7" involved varying the operating temperatures in order to assess the relative stability of this compound with respect to disproportionation to other niobium compounds. Somewhat surprisingly, we discovered a new structure type for the Nb_3YX_7 stoichiometry, which still contains monocapped Nb_3 triangular clusters, yet forms at temperatures lower than ca. 930 K [49]. Crystals of this material were obtained by heating a stoichiometric mixture of the elements under conditions of chemical transport between a temperature gradient of 925–800 K for 2 days.

The resulting compound Nb_3SI_7 crystallizes in an orthorhombic crystal class, space group *Pnma*, and represents another mode of connectivity of the $[Nb_3X_{13}]$ clusters to form a novel two-dimensional structure. As Fig. 8 shows, a layered compound results, but the $^2_\infty[Nb_3SI_7]$ sheets undulate along the crystallographic *ab*-plane. The corresponding structural formula is $[NbS^{i-a}_{1/4}I^i_{2/2}I^{a-a}_{3/2}]_2[NbS^{i-a}_{2/4}I^i_{2/2}I^{a-a}_{2/2}]$, and immediately reveals two inequivalent sets of niobium atoms.

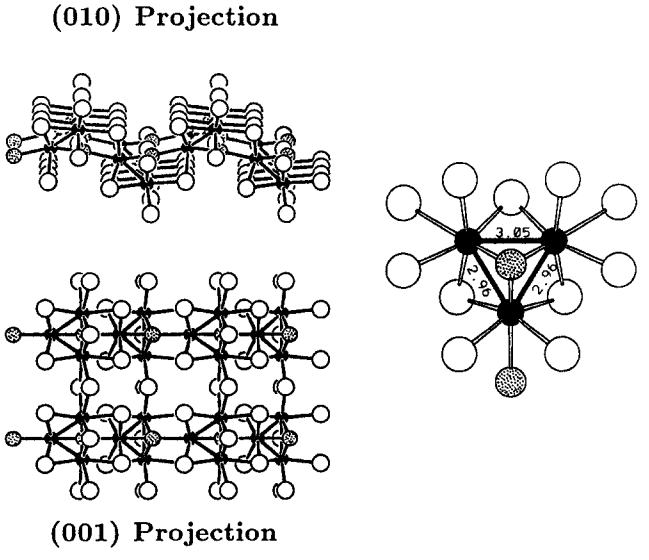

Fig. 8. Left top, (010) perspective view and, left bottom, (001) perspective view of $^2_\infty[o\text{-}Nb_3SI_7]$. Filled circles Nb; dotted circles, S; open circles, I. Right, $[Nb_3S_2I_{11}]^{6-}$ cluster isolated from $o\text{-}Nb_3SI_7$, Nb–Nb distances are indicated. Calculated overlap populations are 0.238 (3.05 Å) and 0.241 (2.96 Å).

Although the Nb_3 clusters are six-electron triangles (closed subshell configurations according to Fig. 4), the symmetry of the cluster is now C_s (not C_{3v}) with two short Nb–Nb bonds and one long Nb–Nb bond. This structural feature has origins in the electronic structure of the $[Nb_3S_2I_{11}]^{6-}$ fragment that takes into account the different ligands on the extremities of the cluster. One Nb atom is coordinated to two sulfur atoms that are trans to one another. A simple angular overlap model quickly rationalizes that two π donors coordinated to a d^2 metal ion should adopt the trans configuration. The Nb–Nb bond length differences occur as the bonding electron density becomes polarized in the Nb_3 triangle towards the unique Nb atom. Nb–Nb overlap populations for these two bonds in an idealized $[Nb_3S_2I_{11}]^{6-}$ cluster correlate with the observed bond lengths (see Fig. 8). This polarization occurs because the sulfide ligand is a stronger π donor than the iodide ligand [49].

The coordination of sulfur by Nb atoms may be derived from an octahedral geometry and can be described as distorted cis-divacant; a coordination mode observed in $Sc_{1-x}S$ [50]. Furthermore, this local geometry contributes to the undulating layered structure of this orthorhombic phase. Careful examination of the complete structure reveals a cubic close-packed arrangement of S^{2-} and I^- anions with Nb atoms in 3/8 of the octahedral holes. In fact, the distribution of Nb atoms along the stacking direction of the anion packing reveals a concentration wave consisting of alternating 5/8 and 1/8 occupation of the octahedral holes. Furthermore, the distribution of sulfur atoms seems to maximize their mutual separation within the anion packing. Electronic structure calculations, however, suggest that this structure is energetically disfavored with respect to the Nb_3X_8-type arrangement.

5.2. Stabilization of monomeric NbI_5

Our attempts to try different transport conditions by introducing excess iodine as a transport agent led to the discovery of another new Nb–S–I phase with stoichiometry $Nb_7S_2I_{19}$ [51]. This compound could, in fact, be obtained in nearly quantitative yield by heating a stoichiometric mixture of the elements at 1100 K in a small fused-silica ampoule for 2 days. Remarkably, this compound has two unique structural components: (1) another novel $^2_\infty[Nb_3SI_7]$ two-dimensional network incorporating Nb_3 triangles; (2) inserted NbI_5 molecules (see Fig. 9). Our structural analysis required solution and refinement from twinned crystal data. During the initial stages of refinement, we detected systematic deviations for reflections with $h = 6n$, $n = 0, 1, 2, \ldots$. The lattice metrics do provide a geometrical condition for twinning that creates problems for analysis of these reflections. Fig. 10 illustrates how a

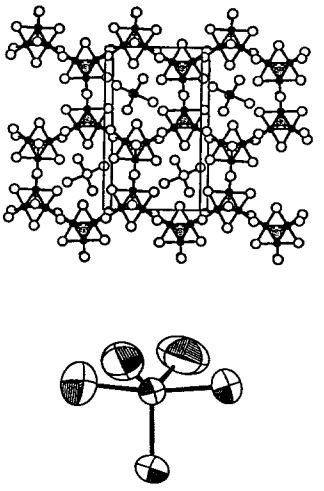

Fig. 9. Top, (010) Projection of $Nb_7S_2I_{19} \equiv [Nb_3SI_7]_2 \cdot NbI_5$ and bottom, (010) projection of an NbI_5 molecule in $Nb_7S_2I_{19}$ (90% displacement ellipsoids): filled circles, Nb; dotted circles, S; open circles, I.

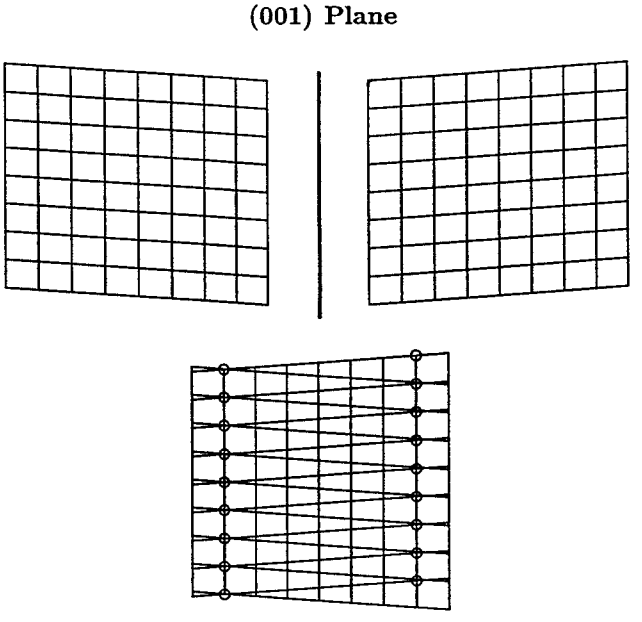

Fig. 10. Two (010) reciprocal lattice planes of monoclinic $Nb_7S_2I_{19}$ related by a mirror plane perpendicular to the c axis. They are shown superimposed and the overlapping reflections ($h = 6n$) are circled.

mirror plane, which relates one crystalline individual with another, leads to complete overlap of the $h = 6n$ reflections when the two corresponding reciprocal lattice planes are superimposed. Therefore, during our solution, we initially omitted these reflections, which allowed successful refinement of the structure. Once a working model was in place, we could then include these reflections and obtain a ratio of the two individuals that led to excellent agreement with the observed diffraction pattern.

This beautiful structure (see Fig. 9) consists of bicapped Nb_3 triangular clusters that are interconnected to form a graphite-type nearly hexagonal net. The structural formula is $2[NbS^{i}_{1/3}I^{i}_{1/3}I^{i}_{2/2}I^{a-a}_{2/2}]_3[NbI_5]$. As Fig. 9 suggests, one structural synergism between the $^{2}_{\infty}[Nb_3SI_7]$ layer and the NbI_5 molecules is the formation of a monoclinic lattice, which is only slightly shifted from hexagonal symmetry. In the $^{2}_{\infty}[Nb_3SI_7]$ partial structure, there are again six valence electrons per Nb_3 triangle, which is sufficient to saturate Nb–Nb bonding orbitals, and adopt a structure that is nearly hexagonal. However, since one equatorial Nb–I bond in the NbI_5 unit is parallel to the stacking axis, the highest rotational symmetry allowed is a twofold axis. Furthermore, orthorhombic (*mmm*) symmetry is precluded in order to minimize I···I non-bonded repulsions between the NbI_5 molecules and the $^{2}_{\infty}[Nb_3SI_7]$ framework, which produces at most a monoclinic (2/*m*) lattice.

A structural hierarchy (**4**) [38] gives further insights into the intricacies of the interactions between layer and molecule, as well as highlights reasons for the twinning mechanism to occur, k2 indicates a klassengleiche group–subgroup relation of index 2, and t2 represents a translationengleiche group–subgroup relation of index 2.

$P6/m2/m2m \leftarrow$ Hypothetical Nb_3I_8

$\downarrow$ t3

$C2/m2/m2/m$

$\downarrow k2$

$P2_1/m2_1/m2/n \leftarrow Nb_3SI_7$ layer

$\downarrow k2,\ a,b,2c$

$P2_1/c2_1/c2/n \leftarrow$ Doubled c axis

$\downarrow$ t2

$P12_1/c1 \leftarrow Nb_7S_2I_{19}$

4

If we at first focus attention on the two-dimensional framework, the highest allowed symmetry group for this structure is *P6/mmm* (a hypothetical Nb_3I_8). The pattern with which S replaces I as a capping atom of the Nb_3 clusters produces the orthorhombic cell with symmetry *Pmmn* and the metric relations $a_{ortho} = \sqrt{3}a_{hex}$, $b_{ortho} = a_{hex}$, and $c_{ortho} = c_{hex}$. Doubling along the *c* axis produces the subgroup *Pccn*, and then introducing the NbI_5 monomers so that one $Nb–I_{eq}$ bond lies parallel to *c* lowers the space group to $P2_1/c$ via a t2 step. The resulting monoclinic cell is given by

$$a_{mono} \sim b_{ortho} = a_{2,hex}$$
$$b_{mono} \sim a_{ortho} = 2a_{1,hex} - a_{2,hex}$$
$$c_{mono} \sim c_{ortho} = 2c_{hex}$$

Since there are two possible orientations of the trigonal bipyramid with respect to the mirror plane perpendicular to the a_{mono} axis, twinning results.

The other component in the structure of $Nb_7S_2I_{19}$ is a trigonal bipyramidal monomer of NbI_5. These molecular entities pack between the Nb_3SI_7 layers within nearly hexagonal channels along the *c* axis. In the solid state, brass-colored NbI_5 has been reported to form complex chains of cis-vertex-sharing octahedra, $NbI_4I_{2/2}$ [11], which differ from the chains of trans-edge-sharing octahedra in $NbCl_5$ and $NbBr_5$ [3,7]. However, only the I positions and not the Nb positions were determined, so that another solution involving Nb_2I_{10} molecules is also possible [52]. Electron diffraction studies on the vapors of $NbCl_5$ and $NbBr_5$ indicate trigonal bipyramidal geometries [53], but NbI_5 is thermally unstable, and decomposes into reduced niobium iodides ($NbI_5(g) \rightarrow NbI_4(g) + 1/2I_2(g)$) [54]. To our knowledge, this is the first example of monomeric NbI_5 molecules in the solid state. The average Nb–I distance of 2.671(6) Å is consistent with a higher formal oxidation state for these Nb atoms than those in the $^{2}_{\infty}[Nb_3SI_7]$ framework ($\langle Nb–I \rangle_{av} = 2.780(5)$ Å). In addition, there is an excellent correlation between Nb–X distances (X ≡ Cl [3], Br [7], I) in NbX_5 and the ionic radii of X^-. A revised value of $r(Nb^{5+})$ based on these data is 0.51 Å.

5.3. Miscibility between Nb_3SI_7 and Nb_3I_8

The similarity in electronegativity between sulfur and iodine led us to examine sequential substitution of I by S in Nb_3I_8. The $\mu^3 - X^i$ anion capping the Nb_3 cluster is where substitution takes place exclusively. This series of experiments revealed a clear dependence of three-dimensional morphology on the identity of the anionic packing [49]. For the sulfur-rich region, the non-centrosymmetric space group is adopted, whereas for the iodine-rich region the centrosymmetric rhombohedral structure is found. From single-crystal analyses carried out at room temperature, we have not detected any long-range ordering of sulfur or iodine, either within a two-dimensional sheet or from one layer to another. There are two important effects to consider as this substitution takes place: (1) the matrix effect due to differing ionic or atomic radii; (2) the electronic effect due to the differing charge requirements. The matrix effect dominates the observed trends in lattice parameters *a*, *c*, and of course unit cell volume. Both matrix and electronic effects, however, are influential for local effects, i.e. cluster metrics. Sulfur-capped clusters are six-electron units; iodine-capped clusters are seven-electron units. Since we have identified the HOMO in Nb_3I_8 to be slightly Nb–Nb bonding, matrix and electronic effects counteract one another to give nearly constant Nb–Nb distances along the series (see Table 4). Moreover, the

Table 4
Structural and magnetic characteristics of $Nb_3S_{1-x}I_{7+x}$ $(0 \leq x \leq 1)$

Compound	Space Group	Volume (Å^3)	Nb–Nb (Å)	Nb–S (Å)	Nb–I (Å)	μ_{eff} ($T > 20$ K)	Θ (K)
Nb_3SI_7	$P6_3mc$	336.32	2.995	2.404	2.737–2.993	—	—
$Nb_3S_{0.67}I_{7.33}$	$P6_3mc$	340.69	2.989	2.426	2.575–3.027	0.24	−3.7(1)
$Nb_3S_{0.33}I_{7.67}$	$R\bar{3}m$	344.30	2.993	2.460	2.736–3.037	0.23	−10.3(3)
Nb_3I_8	$R\bar{3}m$	348.29	3.002	—	2.755–3.020	0.32	−10.1(3)

stronger orbital interactions between Nb and S push the LUMO of Nb_3SI_7 above the HOMO of Nb_3I_8 such that they have similar Fermi levels (chemical potentials). These local effects rationalize the quasicontinuous change in composition in $Nb_3S_{1-x}I_{7+x}$ from $x = 0$ to $x = 1$.

Magnetic susceptibility measurements on these compounds are particularly interesting and are currently undergoing scrutiny. Our preliminary data are summarized in Table 4. All except Nb_3SI_7 are paramagnetic but with extremely low effective magnetic moments. The follow a Curie–Weiss dependence between 50 and 300 K, but the nature of inter luster exchange interactions is not well understood. A superexchange mechanism via the bridging halides is currently postulated as the cause of these reduced moments. Neutron diffraction experiments are currently underway to examine these phenomena in more detail.

6. Metal–organic precursors

Another growing part of our research efforts involves searching for organometallic compounds that may serve as either single-source precursors for chemical vapor deposition growth of binary metal chalcogenides or as soluble species that will allow for low temperature synthesis of novel chalcogenides and chalcogenide halides. After the recent report of the modified Fischer–Hafner synthesis of bis-arene transition metal(0) compounds [55], we have been using bis-mesitylene niobium and molybdenum as starting reagents toward the production of novel chalcogenides and halides. These organometallic reagents also provide reactions and compounds that help us understand the overall cluster chemistry of these elements.

(η^6-mesitylene)$_2$Nb and (η^6-mesitylene)$_2$Mo (mesitylene is $C_6H_3(CH_3)_3 \equiv$ mes) can be synthesized in nearly 50% yield via reduction of $NbCl_5$ by aluminum. Both are monomeric complexes in solution as well as in their crystalline solids. (η^6-mes)$_2$Mo is a pale green, diamagnetic, 18-electron complex and (η^6-mes)$_2$ Nb is a deep red, paramagnetic, 17-electron complex. Both complexes react with halogens: the Mo compound gives monomeric (η^6-mes)$_2$MoX [56], whereas (η^6-mes)$_2$Nb produces diamagnetic dimers [(η^6-mes)Nb]$_2$X$_4$ [55,57]. The cluster complexes involve an Nb–Nb dimer quadruply bridged by iodide ions. The mesitylene ligand is significantly distorted from planarity and shows shifts in the C–C bond distances towards localization of π electron density within the six-membered ring. These d^2–d^2 Nb_2 dimers can be oxidized chemically or electrochemically to give an isostructural $d^{2.5}$–$d^{2.5}$ intermediate valent Nb_2 complex [57]. One unpaired electron is demonstrated by magnetic susceptibility measurements, and its delocalization through the [Nb_2I_4] core is seen in electron paramagnetic resonance spectra.

We have used these two molecular complexes as reactants in the low temperature synthesis of chalcogenide solids. Examples of such syntheses we have carried out include

$$(\eta^6\text{-mes})_2\text{Nb} + 4\text{TePEt}_3 \xrightarrow[210\text{ K}]{\phi\text{Me/PEt}_3} \text{NbTe}_{4(\text{s,amor})} \xrightarrow{400\text{ K}} \text{NbTe}_{4(\text{s,crys})}$$

$$(\eta^6\text{-mes})_2\text{Nb} + \tfrac{1}{4}\,\text{S}_8 \xrightarrow[210\text{ K}]{\text{THF}} \text{NbS}_{1.8(\text{s,amor})} \xrightarrow{800\text{ K}} \text{“r-NbS}_{2(\text{s,crys})}\text{”}$$

$$(\eta^6\text{-mes})_2\text{MO} + \tfrac{1}{4}\,\text{S}_8 \xrightarrow[298\text{ K}]{\text{THF}} \tfrac{1}{2}\,\text{Mo}_2\text{S}_{3(\text{s,amor})} + \tfrac{1}{8}\,\text{S}_8 \xrightarrow{1100\text{ K}} \text{Mo}_2\text{S}_{3(\text{s,amor})}$$

$$(\eta^6\text{-mes})_2\text{Mo} + \tfrac{3}{8}\,\text{S}_8 \xrightarrow[210\text{ K}]{\text{THF}} \text{MoS}_{2.1(\text{s,amor})} \xrightarrow{1000\text{ K}} \text{“r-MoS}_{2(\text{s,crys})}\text{”}$$

Reactions are generally “instantaneous”, and the products are analyzed by elemental analysis and X-ray power diffraction. Investigations are still underway to probe the reaction mechanisms and intermediates that occur.

Recent efforts have concentrated on single-source precursors for chemical vapor deposition of thin film dichalcogenides. Since CH_3S–SCH_3 and I_2 are isoelectronic and isolobal, we have been successful in isolating a metal–organic compound that contains an [Nb_2S_4] core [58,59], a potential single-source precursor for NbS_2. The reaction is carried out analogously to the halogen reactions and produces the dimer [(η^6-mes)Nb]$_2$(SCH$_3$)$_4$. Pyrolysis of this dimeric complex gives an amorphous product which analyzes as $NbS_{1.56}$, and brief annealing of the product at

1100 K leads to crystalline materials whose X-ray powder pattern resembles r-NbS_2.

7. Summary

The cluster chemistry of niobium halides and the solid state chemistry of early transition metal chalcogenides enjoy a rich history and have been well developed, but the combination of these two areas is leading to a bounty of new structures, new synthetic approaches, and eventually exciting chemical and physical properties. Detailed investigations into the Nb–S–I ternary phase diagram reveal many new and exciting phenomena to be discovered and examined in the general niobium–chalcogen phase field. Our work is only scratching the surface, and the potential chemistry of this entire area remains to be explored.

Acknowledgements

The work reported in this contribution could not have been possible without the efforts and suggestions of Jianhua Lin, Myungok Yoon, Mark Smith, Chi-Shen Lee, Jerry A. Ostenson, Wolfgang Hönle, Sigrid Furuseth, and Arndt Simon. R.A. Jacobson has generously provided use of diffractometers. This research is supported both by the Chemical Sciences Division, Office of basic Energy Sciences, US Department of Energy, under Contract W-7405-Eng-82 and the Donors of the Petroleum Research Fund, administered by the American Chemical Society.

References

[1] R.J. Angelici, in R.B. King (ed.), *Encyclopedia of Inorganic Chemistry*, Vol. 3, Wiley, New York, 1994, p. 1433.
[2] H. Schäfer and H.G. von Schnering, *Angew. Chem., 76* (1964) 833.
G.J. Miller, in R.B. King (ed.), *Encyclopedia of Inorganic Chemistry*, Vol. 3, Wiley, New York, 1994, p. 1433.
[3] W. Hönle and H.G. von Schnering, *Z. Kristallogr., 191* (1990) 139.
[4] D.L. Kepert and R. Mandyczewsky, *Inorg. Chem. 7* (1968) 2091.
[5] H.G. von Schnering, H. Wöhrle and H. Schäfer, *Naturwissenschaften 48* (1961) 159.
[6] A. Simon, H.G. von Schnering, H. Wöhrle and H. Schäfer, *Z. Anorg. Allg. Chem., 339* (1965) 155.
[7] U. Müller and P. Klingelhöfer, *Z. Naturforsch., B38* (1983) 559.
[8] S.S. Berdonosov, A.V. Lapitskii and D.G. Berdonosova, *Zh. Neorgan. Khim., 9* (1964) 2569; *Russ. J. Inorg. Chem., 9* (1964) 1388.
[9] S.S. Berdonosov and A.V. Lapitskii, *Zh. Neorgan. Khim., 10* (1965) 2812; *Russ. J. Inorg. Chem., 10* (1965) 1525.
[10] A. Simon and H.G. von Schnering, *J. Less-Common Met., 11* (1966) 31.
[11] W. Littke and G. Brauer, *Z. Anorg. Allg. Chem., 325* (1963) 112.
B. Krebs and D. Sinram, *Z. Naturforsch., B35* (1980) 12.
[12] L.F. Dahl and D.C. Wampler, *Acta Crystallogr., 15* (1962) 903.
[13] P.W. Seabaugh and J.D. Corbett, *Inorg. Chem., 4* (1965) 176.
[14] A. Simon, H.G. von Schnering and H. Schäfer, *Z. Anorg. Allg. Chem., 355* (1967) 295.
H. Imoto and A. Simon, *Inorg. Chem., 21* (1982) 308.
[15] F. Hulliger, in F. Lévy (ed.), *Structural Chemistry of Layer-Type Phases*, Reidel, Dordrecht, 1976.
[16] J. Rouxel, *Comments Inorg. Chem., 14* (1993) 207.
[17] J.E. Huheey, *Inorganic Chemistry*, Harper & Row, New York, 1972, p. 164.
[18] M.J. Martin, G.-H. Qiang and D.M. Schleich, *Inorg. Chem. 27* (1988) 2804.
[19] A. Bensalem and D.M. Schleich, *Mater. Res. Bull. 25* (1990) 349.
[20] H.F. Franzen, W. Hönle and H.G. von Schnering, *Z. Anorg. Allg. Chem., 497* (1983) 13.
[21] J. Rijnsdorp, G.J. de-Lange and G.A. Wiepers, *J. Solid State Chem., 30* (1979) 365.
[22] H.-J. Meyer and J.D. Corbett, *Inorg. Chem., 30* (1991) 963.
[23] J. Rijnsdorp and F. Jellinek, *J. Solid State Chem., 28* (1979) 149.
[24] A. Meerschaut, P. Grenouilleau and J. Rouxel, *J. Solid State Chem., 61* (1986) 90.
[25] A. Meerschaut, P. Grenouilleau, L. Giuemas and J. Rouxel, *J. Solid State Chem., 70* (1987) 36.
[26] P. Grenouilleau, A. Meerschaut, L. Guemas and J. Rouxel, *J. Solid State Chem., 66* (1987) 293.
[27] P. Grenouilleau, A. Meerschaut and J. Rouxel, *Eur. J. Solid State Chem., 25* (1988) 77.
[28] A. Meerschaut, P. Palvadeau and J. Rouxel, *J. Solid State Chem., 20* (1977) 21.
[29] V.E. Fedorov, V.K. Evstaf'ev, S.D. Kirik and A.V. Mishchenko, *Zh. Neorg. Khim., 26* (1981) 2701.
[30] H. Ben-Yaich, J.C. Jegaden, M. Potel, M. Sergent, A.K. Rastogi and R. Tournier, *J. Less-Common Meth. 102* (1984) 9.
[31] W. Tremel, *Inorg. Chem., 31* (1992) 755.
[32] W. Tremel, *Chem. Ber., 125* (1992) 2165.
[33] S.-Q. Deng, H.-H. Zhuang, C.-Z. Lu, J.-S. Huang and J.-L. Huang, *Acta Crystallogr. C, 49* (1993) 1135.
[34] J.D. Corbett, in A.K. Cheetham and P. Day (eds.), *Solid State Chemistry: Techniques*, Clarendon, New York, 1987, p. 1.
[35] H. Schäfer, *Chemical Transport Reactions*, Academic Press, New York, 1964.
[36] N.N. Greenwood and A. Earnshaw, *Chemistry of the Elements*, Pergamon, Oxford, 1984.
[37] H.Y. Chen, R.T. Tuenge and H.F. Franzan, *Inorg. Chem., 12* (1973) 552.
[38] U. Müller, *Inorganic Structural Chemistry*, Wiley, New York, 1992.
[39] D.L. Kepert and R.E. Marshall, *J. Less-Common Met., 34* (1974) 153.
[40] F.A. Cotton, M.P. Diebold, X. Feng and W.J. Roth, *Inorg. Chem., 27* (1988) 3413.
[41] F.A. Cotton and T.E. Haas, *Inorg. Chem., 3* (1964) 10.
B.E. Bursten, F.A. Cotton and G.G. Stanley, *Isr. J. Chem., 19* (1980) 132.
F.A. Cotton, M.B. Hall and R. Najjar, *Inorg. Chem., 21* (1982) 302.
[42] H.-J. Meyer, *Z. Anorg. Allg. Chem., 620* (1994) 81.
[43] G.J. Miller, *J. Alloys Comp., 217* (1995) 5.
[44] D.A. McQuarrie, *Statistical Mechanics*, Harper & Row, New York, 1973.
[45] R. Hoffmann, *Solids and Surfaces: a Chemist's View of Bonding in Extended Structures*, VCH, New York, 1988.

[46] J.K. Burdett, *Prog. Solid State Chem.*, *15* (1984) 173.
B.M. Gimarc, *J. Am. Chem. Soc.*, *105* (1983) 1979.
[47] S. Furuseth, W. Hönle, G.J. Miller and H.G. von Schnering, *9th Int. Conf. on Solid Compounds of Transitions Elements, Abstracts*, Royal Society of Chemistry, London, 1988.
G.J. Miller, S. Furuseth, W. Hönle and H.G. von Schnering, to be published.
[48] G.V. Khvorykh, A.V. Shevelkov, V.A. Dolgikh, B.A. Popovkin, submitted to *Inorg. Chem.*, private communication, 1995.
[49] G.J. Miller and J. Lin, manuscript in preparation.
[50] J.P. Dismukes and J.G. White, *Inorg. Chem.*, *3* (1964) 1220.
[51] G.J. Miller and J. Lin, *Angew. Chem.*, *106* (1994) 357; *Angew. Chem. Int. Ed. Engl.*, *33* (1994) 334.
[52] U. Müller, *Acta Crystallogr. A*, *34* (1978) 256.
[53] H.A. Skinner and L.E. Sutton, *Trans. Faraday Soc.*, *36* (1940) 668.
[54] J.H. Canterford and R. Colton, *Halides of the Second and Third Row Transition Metals*, Wiley-Interscience, London, 1968, pp. 154, 161.
[55] F. Calderazzo, G. Pampaloni, L. Rocchi, J. Strähle and K. Wurst, *Angew. Chem. Int. Ed. Engl.*, *30* (1991) 102.
[56] E.O. Fischer and H.O. Stahl, *Chem. Ber.*, *93* (1960) 2065.
[57] M. Yoon, J. Lin, V.G. Young, G.J. Miller, submitted to *J. Organomet. Chem.*, 1994.
[58] M. Yoon and G.J. Miller, unpublished research.
[59] M.L.H. Green, D. O'Hare, P. Mountford and J.G. Watkin, *J. Chem. Soc. Dalton Trans.*, (1991) 1705.